AIAA Guidance, Navigation, and Control Conference
2 - 5 August 2010, Toronto, Ontario Canada

AIAA 2010-7885

Downloaded by TECHNISCHE UNIVERSITEIT DELFT on December 30, 2013 | http://arc.aiaa.org | DOI: 10.2514/6.2010-7885

Relative Orbital Element Estimation and Observability Analysis for Formation Flying Satellites using Inter-Satellite Range Measurements Only

Daan C. Maessen[1] and Eberhard Gill[2]
Delft University of Technology, Faculty of Aerospace Engineering, 2629 HS, Delft, The Netherlands

This paper investigates to what extent the relative orbital elements of two satellites flying in formation can be estimated making use of inter-satellite range measurements only. Since the determination of relative orbital elements does not require the orientation of the relative orbit with respect to absolute inertial space to be resolved, as would be the case for absolute orbital elements, the question arises whether relative range measurements alone can be sufficient to solve the problem of interest. Providing an answer to this question is both of academic and practical interest, especially for formation flying missions utilizing very small satellites that are limited in their capabilities. To this end, a linearized relative dynamics model is implemented using an iterative batch least-squares algorithm to estimate rectilinear relative positions and velocities, which are subsequently converted to relative orbital elements for a number of test cases. Furthermore, the observability of the system is analyzed to investigate which relative orbital elements are most observable.

Nomenclature

Roman Symbols

$\boldsymbol{A}$ = state matrix
a = semi-major axis
a_x, a_y, a_z = perturbing accelerations in x-, y-, or z-direction
$\mathrm{Cov}(\cdot,\cdot)$ = covariance
c = cosine function
du = mean argument of latitude difference
$\boldsymbol{e}$ = relative eccentricity vector
e = eccentricity
e_x, e_y = eccentricity vector entries
$\boldsymbol{G}$ = Gramian matrix
$\boldsymbol{H}$ = partial derivatives matrix
$\boldsymbol{h}$ = vector containing the modeled measurements
$\boldsymbol{i}$ = relative inclination vector
i = inclination
i_x, i_y = inclination vector entries
j = number of iterations
M = mean anomaly
m = number of observations
n = orbital mean motion
$\boldsymbol{o}$ = Hill frame unit vector
$\boldsymbol{P}$ = covariance matrix
$\boldsymbol{r}$ = relative position vector in Hill coordinates
r = inter-satellite range
s = sine function
t = time

---

[1] Ph.D. Candidate, Department of Space Engineering, d.c.maessen@tudelft.nl, AIAA Student Member.
[2] Professor Space Systems Engineering, Department of Space Engineering, e.k.a.gill@tudelft.nl.

Copyright © 2010 by D.C. Maessen. Published by the American Institute of Aeronautics and Astronautics, Inc., with permission.

Downloaded by TECHNISCHE UNIVERSITEIT DELFT on December 30, 2013 | http://arc.aiaa.org | DOI: 10.2514/6.2010-7885

$\boldsymbol{U}$ = orthonormal matrix of a singular value decomposition
u = mean argument of latitude
$\boldsymbol{V}$ = eigenvector matrix
$\boldsymbol{v}$ = relative velocity vector in Hill coordinates
$\boldsymbol{x}$ = relative state vector in Hill coordinates
$\dot{\boldsymbol{x}}$ = time derivative of the relative state vector in Hill coordinates
x, y, z = relative radial, along-track and cross-track position in the Hill frame
$\dot{x}, \dot{y}, \dot{z}$ = relative radial, along-track and cross-track velocity in the Hill frame
$\ddot{x}, \ddot{y}, \ddot{z}$ = relative radial, along-track and cross-track acceleration in the Hill frame
$\boldsymbol{z}$ = measurement vector

Greek symbols
$\boldsymbol{\Gamma}$ = transformation matrix
Δ = difference operator
δ = orbital element difference operator
$\delta\boldsymbol{\alpha}$ = relative orbital elements vector
θ = phase of the relative inclination vector
κ = condition number of the singular value matrix $\boldsymbol{\Sigma}$
$\boldsymbol{\Lambda}$ = information matrix
λ = mean longitude
μ = Earth's gravitational constant
ρ = inter-satellite pseudorange
ρ_{ab} = correlation between 'a' and 'b'
$\boldsymbol{\Sigma}$ = singular value matrix
Σ = singular value
σ = (co-)variance
$\boldsymbol{\Phi}(t,0)$ = state transition matrix from $t = 0$ to t
φ = phase of the relative eccentricity vector
Ω = right ascension of the ascending node
ω = argument of perigee

Subscripts
0 = initial epoch
d = deputy satellite
nt = product $n \cdot t$ acting as cosine or sine function argument
u = mean argument of latitude u acting as cosine or sine function argument
x, y, z = relative radial, along-track and cross-track position in the Hill frame
$\dot{x}, \dot{y}, \dot{z}$ = relative radial, along-track and cross-track velocity in the Hill frame

Superscripts
apr = a priori
lsq = least-squares solution
ref = reference state
* = adapted matrix

I. Introduction

In the field of satellite formation flying, it is of key interest to reduce ground operations efforts as this may limit mission functionality due to visibility restrictions and may drive mission costs. Thus, the formation has to handle as many tasks as necessary autonomously. One task that lends itself well to this is the guidance, navigation and control of the formation

As pointed out by D'Amico and Montenbruck[1], formation flying satellites are able to autonomously control the formation geometry when the relative orbital elements of the satellites are known. Expression of the formation geometry using relative orbital elements namely allows the use of Gauss' variational equations, adapted to near-circular non-equatorial orbits, for formation control. As these equations provide the change of the relative orbital

Downloaded by TECHNISCHE UNIVERSITEIT DELFT on December 30, 2013 | http://arc.aiaa.org | DOI: 10.2514/6.2010-7885

elements due to an impulsive thrust in a certain direction and at a certain location, they are an excellent tool to solve the maneuver planning problem[1].

To increase the autonomy of the formation, the relative orbital elements can be obtained using onboard sensors that sense either the relative positions or the absolute positions (e.g. using GPS) of the satellites in the formation. Studies carried out by Markley[2], Psiaki[3], Yim et al.[4], Doolittle et al.[5], Woffinden and Geller[6,7], and Kang et al.[8] for autonomous (relative) orbit determination of multiple satellites have assumed that relative line-of-sight and possibly relative range measurements are available from onboard sensors. Chavez and Lovell[9] limited the sensor information to only inter-satellite range measurements, but the cases they considered were limited to in-plane motions only.

The objective of this work is to investigate to what extent the relative orbital elements of two satellites flying in formation in a low Earth orbit (LEO) can be estimated using a linearized relative dynamics model and inter-satellite range measurements only. Throughout the paper, the satellite denoted as the 'chief' is assumed to have a circular orbit. The other satellite will be denoted as the 'deputy'. The satellites perform inter-satellite range measurements using a locally generated radiofrequency ranging signal. As the fundamental properties of the problem are to be analyzed, a most simple case is set up. The deputy satellite uses a single antenna to transmit the ranging signal to the chief satellite, which uses one receiver antenna to pick up the signal and determine the relative range. It is further assumed that the location of the antennas coincides with the center of mass of the satellites, which implies that relative line-of-sight measurements cannot be performed. It is assumed that the range measurements are perfect. The range measurements are treated together with a dynamic model of the satellites' relative motion to estimate their relative orbit using an iterative batch least-squares algorithm. This estimator has been selected over sequential filters to eliminate process noise buildup for long observation arc lengths. Several test cases are investigated and their results are discussed.

II. Orbital Dynamics Modeling

Since the relative orbital elements of two co-orbiting satellites are to be determined, an appropriate coordinate frame in which the relative motion can be described is the Hill frame[10]. This frame is centered at the chief spacecraft with the radial unit vector $\boldsymbol{o}_x$ aligned with the orbit radius vector, the normal unit vector $\boldsymbol{o}_z$ aligned with the orbit angular momentum vector, and the tangential unit vector $\boldsymbol{o}_y$ directed such that a right-handed Cartesian reference frame is formed. The relative motion of the deputy with respect to the chief is expressed through Hill coordinates as

$$\boldsymbol{x} = \begin{pmatrix}\boldsymbol{r} & \boldsymbol{v}\end{pmatrix}^T = \left(x,\ y,\ z,\ \dot{x},\ \dot{y},\ \dot{z}\right)^T \tag{1}$$

where the vectors $\boldsymbol{r}$ and $\boldsymbol{v}$ denote the relative positions $\left(x, y, z\right)^T$ and velocities $\left(\dot{x}, \dot{y}, \dot{z}\right)^T$, respectively.

A. Clohessy-Wiltshire

In case of a Keplerian two-body motion, a circular chief orbit, and spacecraft separations much smaller than the chief's semi-major axis, the Clohessy-Wiltshire (CW) equations can be used to express the linearized relative spacecraft dynamics in the Hill frame[11]:

$$\begin{aligned} \ddot{x} - 2n\dot{y} - 3n^2 x &= a_x \\ \ddot{y} + 2n\dot{x} &= a_y \\ \ddot{z} + n^2 z &= a_z \end{aligned} \tag{2}$$

with $\ddot{x}, \ddot{y}, \ddot{z}$ denoting relative accelerations, a_i perturbing accelerations in x-, y-, or z-direction and n the orbital mean motion of the chief satellite, which is defined as

$$n = \sqrt{\frac{\mu}{a^3}} \tag{3}$$

with μ the Earth's gravitational constant and a the semi-major axis. We are interested in the homogeneous solution to this set of equations and can therefore set the perturbing accelerations to zero, allowing us to rewrite Eq. (2) as

$$\dot{\boldsymbol{x}}(t) = \boldsymbol{A}\boldsymbol{x}(t) \tag{4}$$

or

$$\begin{pmatrix} \dot{x} \\ \dot{y} \\ \dot{z} \\ \ddot{x} \\ \ddot{y} \\ \ddot{z} \end{pmatrix} = \begin{pmatrix} 0 & 0 & 0 & 1 & 0 & 0 \\ 0 & 0 & 0 & 0 & 1 & 0 \\ 0 & 0 & 0 & 0 & 0 & 1 \\ 3n^2 & 0 & 0 & 0 & 2n & 0 \\ 0 & 0 & 0 & -2n & 0 & 0 \\ 0 & 0 & -n^2 & 0 & 0 & 0 \end{pmatrix} \begin{pmatrix} x \\ y \\ z \\ \dot{x} \\ \dot{y} \\ \dot{z} \end{pmatrix} \tag{5}$$

Since the state matrix $\boldsymbol{A}$ is time invariant, the state transition matrix $\boldsymbol{\Phi}(t,0)$, mapping the state at time $t_0 = 0$ to the state at time t, is easily obtained using the matrix exponential[11]

$$\boldsymbol{\Phi}(t,0) = e^{At} = \begin{pmatrix} 4-3c_{nt} & 0 & 0 & s_{nt}/n & \dfrac{2(1-c_{nt})}{n} & 0 \\ 6(s_{nt}-nt) & 1 & 0 & \dfrac{2(c_{nt}-1)}{n} & \dfrac{4s_{nt}}{n}-3t & 0 \\ 0 & 0 & c_{nt} & 0 & 0 & \dfrac{s_{nt}}{n} \\ 3ns_{nt} & 0 & 0 & c_{nt} & 2s_{nt} & 0 \\ 6n(c_{nt}-1) & 0 & 0 & -2s_{nt} & 4c_{nt}-3 & 0 \\ 0 & 0 & -ns_{nt} & 0 & 0 & c_{nt} \end{pmatrix} \tag{6}$$

with c_{nt} equal to cos(nt) and s_{nt} equal to sin(nt). Now, the system's evolution can be described as

$$\boldsymbol{x}(t) = \boldsymbol{\Phi}(t,0)\,\boldsymbol{x}(0)\,. \tag{7}$$

B. Relative Orbital Elements

Just as the description of a satellite's absolute orbit using rectilinear positions and velocities often provides little insight into the geometry of the orbit, so do the CW equations often provide little insight into the geometry of the formation. Describing an absolute satellite orbit through six Kepler elements, of which five out of six are constant for Keplerian motion, allows a simple geometric representation. For this reason, representations have been developed that express the relative motion of two satellites in terms of relative orbital elements. Following Ref. 12, the relative motion of two closely spaced satellites is expressed in relative orbital elements as

$$\delta\boldsymbol{\alpha} = \begin{pmatrix} \delta a \\ \delta e_x \\ \delta e_y \\ \delta i_x \\ \delta i_y \\ \delta u \end{pmatrix} = \begin{pmatrix} (a_d - a)/a \\ e_{xd} - e_x \\ e_{yd} - e_y \\ i_d - i \\ (\Omega_d - \Omega)\sin i \\ u_d - u \end{pmatrix}. \tag{8}$$

Here, the subscript d refers to the deputy and the δ operator denotes orbital element difference. Furthermore, a is the semi-major axis, e is the eccentricity, i is the inclination, Ω is the right ascension of the ascending node, and u is the mean argument of latitude, which is equal to the sum of the argument of perigee and the mean anomaly ($u = \omega + M$). Note that Ref. 12 uses the relative mean longitude $\delta\lambda$ instead of δu. This representation is based on the concept of relative eccentricity and inclination vectors which are expressed as[1]

$$\delta\boldsymbol{e} = \delta e\begin{pmatrix} \cos\varphi \\ \sin\varphi \end{pmatrix} \text{ and } \delta\boldsymbol{i} = \delta i\begin{pmatrix} \cos\theta \\ \sin\theta \end{pmatrix}. \tag{9}$$

Downloaded by TECHNISCHE UNIVERSITEIT DELFT on December 30, 2013 | http://arc.aiaa.org | DOI: 10.2514/6.2010-7885

Downloaded by TECHNISCHE UNIVERSITEIT DELFT on December 30, 2013 | http://arc.aiaa.org | DOI: 10.2514/6.2010-7885

The amplitudes of the relative *e*/*i*-vectors are denoted by δe and δi respectively while the phases of the relative *e*/*i*-vectors are denoted by φ and θ. Note that the relative orbital elements of $\delta\boldsymbol{\alpha}$ have dimensionless or angular quantities and that

$$\begin{array}{lll} \delta e_x = e_d \cos\omega_d - e\cos\omega \ , & \delta e = \sqrt{\left(\delta e_x\right)^2 + \left(\delta e_y\right)^2} \ , & \varphi = \mathrm{atan}\left(\dfrac{\delta e_y}{\delta e_x}\right) \\ \delta e_y = e_d \sin\omega_d - e\sin\omega \ , & \delta i = \sqrt{\left(\delta i_x\right)^2 + \left(\delta i_y\right)^2} \ , & \theta = \mathrm{atan}\left(\dfrac{\delta i_y}{\delta i_x}\right) \end{array} . \tag{10}$$

Using the mean argument of latitude u as independent variable and assuming small $\delta\boldsymbol{\alpha}$ components ($\delta\boldsymbol{\alpha} << 1$), a first-order mapping between Hill coordinates and relative orbital elements can be performed that provides the dimensionless relative Cartesian position vector $\boldsymbol{r}/a$ as a function of the relative orbital elements $\delta\boldsymbol{\alpha}$

$$\begin{array}{l} x/a = \delta a - \delta e\cos\left(u-\varphi\right) \\ y/a = \delta\lambda - 3/2\,\delta a\left(u-u_0\right) + 2\delta e\sin\left(u-\varphi\right) . \\ z/a = \delta i\sin\left(u-\theta\right) \end{array} \tag{11}$$

In the above set of equations, u_0 is the mean argument of latitude at the initial time t_0 and $\delta\lambda$ is the relative mean longitude defined as

$$\delta\lambda = \left(u_d - u\right) + \left(\Omega_d - \Omega\right)\cos i \ . \tag{12}$$

Differentiating Eq. (11) with time provides the equations for the relative velocities. Doing this and rewriting gives

$$\begin{pmatrix} x \\ y \\ z \\ \dot{x} \\ \dot{y} \\ \dot{z} \end{pmatrix} = \begin{pmatrix} 1 & -c_u & -s_u & 0 & 0 & 0 \\ -\frac{3}{2}du & 2s_u & -2c_u & 0 & \cot i & 1 \\ 0 & 0 & 0 & s_u & -c_u & 0 \\ 0 & ns_u & -nc_u & 0 & 0 & 0 \\ -\frac{3}{2}n & 2nc_u & 2ns_u & 0 & 0 & 0 \\ 0 & 0 & 0 & nc_u & ns_u & 0 \end{pmatrix} \begin{pmatrix} a\delta a \\ a\delta e_x \\ a\delta e_y \\ a\delta i_x \\ a\delta i_y \\ a\delta u \end{pmatrix} \tag{13}$$

with $du = u - u_0$, $c_u = \cos(u)$ and $s_u = \sin(u)$.

In case $\delta a = 0$ and $\delta u = -(\Omega_d - \Omega)\cos(i)$, the resulting relative motion is completely determined by the amplitude and phase of the relative *e*/*i*-vectors, cf. Fig. 1. If $\varphi = \theta$, an intrinsically safe *e*/*i*-vector separation is achieved since the minimum cross-track separation between the two spacecraft is now min($a\delta e$,$a\delta i$), which is never (0,0)[13].

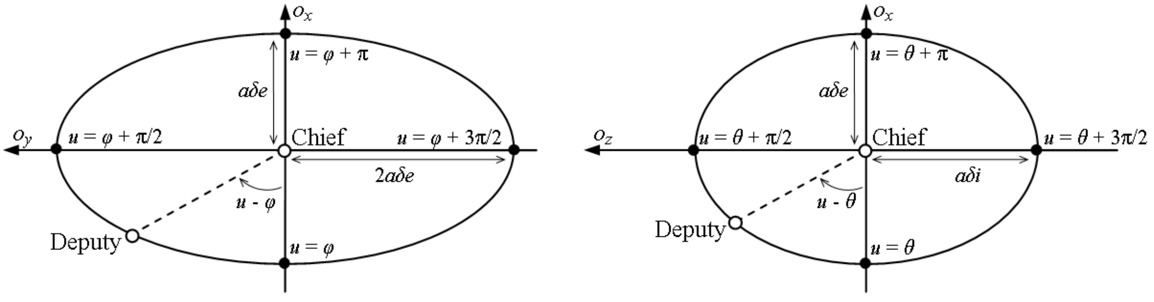

Figure 1. Relative in-plane (left) and out-of-plane (right) motion of the deputy with respect to the chief with e/i-vector separation in the Hill frame, after Ref. 13.

III. Batch Least-Squares Algorithm

An iterative batch leas-squares algorithm is used to estimate the relative state vector $\boldsymbol{x}$ of the two satellites at time t_0. The estimator setup and outputs are described in the next subsections.

A. Estimator Setup

The observed inter-satellite range r at time t is modeled as the Euclidian norm of the relative position vector. The measured inter-satellite pseudorange ρ at time t is assumed to be perfect, giving

$$\rho(t) = r(t) = \left\|\boldsymbol{r}(t)\right\| = \sqrt{x^2(t) + y^2(t) + z^2(t)}\ . \tag{14}$$

The measurements are collected in the measurement vector $\boldsymbol{z}$. Using a linearized relationship between the measurements and state vector $\boldsymbol{x}$

$$\Delta\boldsymbol{z} = \boldsymbol{H}\Delta\boldsymbol{x} \tag{15}$$

with

$$\begin{aligned} &\Delta\boldsymbol{z} = \boldsymbol{z} - \boldsymbol{h}\left(\boldsymbol{x}^{ref}\right) \\ &\Delta\boldsymbol{x} = \boldsymbol{x} - \boldsymbol{x}^{ref} \\ &\boldsymbol{H} = \left.\frac{\partial\boldsymbol{h}(\boldsymbol{x})}{\partial\boldsymbol{x}}\right|_{\boldsymbol{x}=\boldsymbol{x}^{ref}} \end{aligned} \tag{16}$$

where $\boldsymbol{h}(\boldsymbol{x})$ is the vector containing the modeled measurements as a function of the reference state $\boldsymbol{x}^{\mathrm{ref}}$, the sum of squares of the residual error gets minimized by

$$\Delta\boldsymbol{x} = \left(\boldsymbol{H}^T\boldsymbol{H}\right)^{-1}\boldsymbol{H}^T\Delta\boldsymbol{z}\ . \tag{17}$$

The matrix $\boldsymbol{H}$ contains the partial derivatives of the modeled observations with respect to the instantaneous state:

$$\boldsymbol{H}(t) = \left(\frac{\partial\rho(t)}{\partial x(t)},\ \frac{\partial\rho(t)}{\partial y(t)},\ \frac{\partial\rho(t)}{\partial z(t)},\ 0,\ 0,\ 0\right). \tag{18}$$

Since we are not interested in the instantaneous state but in the state at time t_0, Eq. (15) has to be rewritten as

$$\Delta z_t = \boldsymbol{H}_t\Delta\boldsymbol{x}_t = \boldsymbol{H}_t\boldsymbol{\Phi}(t,0)\Delta\boldsymbol{x}_0 = \boldsymbol{H}_t^*\Delta\boldsymbol{x}_0\ . \tag{19}$$

Here the measurement matrix $\boldsymbol{H}_t$* contains the partial derivatives of the measurements at time t with respect to the state vector at epoch t_0. If the measurements of m observation times $t_0 - t_{m-1}$ are used to determine the state at t_0, the observation model is given by

$$\Delta\boldsymbol{z} = \begin{pmatrix} \Delta z_0 \\ \Delta z_1 \\ \vdots \\ \Delta z_{m-1} \end{pmatrix} = \begin{pmatrix} \boldsymbol{H}_{t_0}\boldsymbol{\Phi}(t_0,0) \\ \boldsymbol{H}_{t_1}\boldsymbol{\Phi}(t_1,0) \\ \vdots \\ \boldsymbol{H}_{t_{m-1}}\boldsymbol{\Phi}(t_{m-1},0) \end{pmatrix}\Delta\boldsymbol{x}_0 = \begin{pmatrix} \boldsymbol{H}_{t_0}^* \\ \boldsymbol{H}_{t_1}^* \\ \vdots \\ \boldsymbol{H}_{t_{m-1}}^* \end{pmatrix}\Delta\boldsymbol{x}_0\ . \tag{20}$$

However, inter-satellite range measurements are known to be insensitive to the orientation of the orbit plane[14], leading to an ill-conditioned normal equations matrix ($\boldsymbol{H}^T\boldsymbol{H}$). In such cases, a priori information can be used to make the normal equations matrix well conditioned again. Then, the least-squares solution is[11]

Downloaded by TECHNISCHE UNIVERSITEIT DELFT on December 30, 2013 | http://arc.aiaa.org | DOI: 10.2514/6.2010-7885

Downloaded by TECHNISCHE UNIVERSITEIT DELFT on December 30, 2013 | http://arc.aiaa.org | DOI: 10.2514/6.2010-7885

$$\boldsymbol{x}_0^{lsq} = \boldsymbol{x}_0^{ref} + \boldsymbol{P}\left(\boldsymbol{\Lambda}\left(\boldsymbol{x}_0^{apr} - \boldsymbol{x}_0^{ref}\right) + \boldsymbol{H}^{*T}\Delta \boldsymbol{z}\right) \tag{21}$$

with the information matrix $\boldsymbol{\Lambda}$ the inverse of the a priori covariance matrix $\boldsymbol{P}^{apr}$, given by

$$\boldsymbol{P}^{apr} = \begin{pmatrix} \sigma_x^{apr\,2} & 0 & 0 & 0 & 0 & 0 \\ 0 & \sigma_y^{apr\,2} & 0 & 0 & 0 & 0 \\ 0 & 0 & \sigma_z^{apr\,2} & 0 & 0 & 0 \\ 0 & 0 & 0 & \sigma_{\dot{x}}^{apr\,2} & 0 & 0 \\ 0 & 0 & 0 & 0 & \sigma_{\dot{y}}^{apr\,2} & 0 \\ 0 & 0 & 0 & 0 & 0 & \sigma_{\dot{z}}^{apr\,2} \end{pmatrix}. \tag{22}$$

The terms on the diagonal are the a priori variances of the state components. The matrix $\boldsymbol{P}$ in Eq. (21) is the covariance matrix of the least-squares estimate and is given by

$$\boldsymbol{P} = \left(\boldsymbol{\Lambda} + \boldsymbol{H}^{*T}\boldsymbol{H}^{*}\right)^{-1}. \tag{23}$$

The term $\boldsymbol{\Lambda}\left(\boldsymbol{x}_0^{apr} - \boldsymbol{x}_0^{ref}\right)$ in eq. (21) serves as a 'constraint' to prevent large deviations from the a priori estimate. When j iterations are performed to improve the estimator result, the above can be expressed as

$$\boldsymbol{x}_0^{j+1} = \boldsymbol{x}_0^{j} + \boldsymbol{P}^{j}\left(\boldsymbol{\Lambda}\left(\boldsymbol{x}_0^{apr} - \boldsymbol{x}_0^{j}\right) + \boldsymbol{H}^{*jT}\Delta \boldsymbol{z}^{j}\right). \tag{24}$$

B. Transformation of Estimator Results

As just described, the estimator determines the relative state at t_0 in Hill coordinates and provides the corresponding covariance matrix $\boldsymbol{P}$. However, we are interested in the relative state expressed in relative orbital elements since this provides more geometrical insight. The conversion to relative orbital elements is done as follows.

Taking the inverse of the 6x6 matrix in Eq. (13) allows determination of the relative orbital elements, resulting in

$$\begin{pmatrix} a\delta a \\ a\delta e_x \\ a\delta e_y \\ a\delta i_x \\ a\delta i_y \\ a\delta u \end{pmatrix} = \begin{pmatrix} 4 & 0 & 0 & 0 & \frac{2}{n} & 0 \\ 3c_u & 0 & 0 & \frac{s_u}{n} & \frac{2c_u}{n} & 0 \\ 3s_u & 0 & 0 & -\frac{c_u}{n} & \frac{2s_u}{n} & 0 \\ 0 & 0 & s_u & 0 & 0 & \frac{c_u}{n} \\ 0 & 0 & -c_u & 0 & 0 & \frac{s_u}{n} \\ 6du & 1 & c_u \cot i & -\frac{2}{n} & \frac{3}{n}du & -\frac{s_u \cot i}{n} \end{pmatrix} \begin{pmatrix} x \\ y \\ z \\ \dot{x} \\ \dot{y} \\ \dot{z} \end{pmatrix}. \tag{25}$$

Without loss of generality, for $u = u_0 = 0$, the above simplifies to

$$\begin{pmatrix} a\delta a \\ a\delta e_x \\ a\delta e_y \\ a\delta i_x \\ a\delta i_y \\ a\delta u \end{pmatrix} = \begin{pmatrix} 4 & 0 & 0 & 0 & \frac{2}{n} & 0 \\ 3 & 0 & 0 & 0 & \frac{2}{n} & 0 \\ 0 & 0 & 0 & -\frac{1}{n} & 0 & 0 \\ 0 & 0 & 0 & 0 & 0 & \frac{1}{n} \\ 0 & 0 & -1 & 0 & 0 & 0 \\ 0 & 1 & \cot i & -\frac{2}{n} & 0 & 0 \end{pmatrix} \begin{pmatrix} x \\ y \\ z \\ \dot{x} \\ \dot{y} \\ \dot{z} \end{pmatrix} = \boldsymbol{\Gamma x} . \tag{26}$$

Since n is assumed to be known (in theory, n (and thus a) can be determined from the period of the inter-satellite range variation, which is equal to the chief's orbital period of $2\pi/n$), five of the six equations above can be solved. If either δu or i is known, then also the last equation can be solved. Here, it is assumed that i is known from ground-based observations.

The rows of the transformation matrix $\boldsymbol{\Gamma}$ in Eq. (26) also give the partial derivatives of the relative orbital elements with respect to the state vector. This allows the determination of the covariance matrix of the relative orbital elements using

$$\mathrm{Cov}\left(a\delta\boldsymbol{\alpha}, a\delta\boldsymbol{\alpha}\right) = \boldsymbol{\Gamma P \Gamma}^T \tag{27}$$

with the units of Cov$(a\delta\boldsymbol{\alpha},a\delta\boldsymbol{\alpha})$ being m^2.

IV. Observability Analysis

According to Ref. 15, an nth-order linear time-varying system is locally observable only if its Gramian $\boldsymbol{G}$ is full rank. For the current system, the Gramian is defined as

$$\boldsymbol{G} = \boldsymbol{H}^{*T}\boldsymbol{H}^{*} . \tag{28}$$

Note that this matrix is the inverse of the covariance matrix without a priori information. Although observability can now be readily determined by computing the rank of $\boldsymbol{G}$, this does not provide much insight: The system is either observable or not. Therefore, a singular value decomposition (SVD) of $\boldsymbol{G}$ is performed to obtain more insight in the observability of the system. However, before this is done, the units of the entries in $\boldsymbol{G}$ need to be normalized. Denoting $\boldsymbol{G}$ as

$$\boldsymbol{G} = \begin{pmatrix} \boldsymbol{G}_{\mathrm{rr}} & \boldsymbol{G}_{\mathrm{rv}} \\ \boldsymbol{G}_{\mathrm{vr}} & \boldsymbol{G}_{\mathrm{vv}} \end{pmatrix} \tag{29}$$

and multiplying the 3x3 submatrices $\boldsymbol{G}_{rv}$ and $\boldsymbol{G}_{vr}$ by n and the submatrix $\boldsymbol{G}_{vv}$ by n^2 results in a new Gramian, $\boldsymbol{G}^*$, with units m^{-2}

$$\boldsymbol{G}^* = \begin{pmatrix} \boldsymbol{G}_{\mathrm{rr}} & n\boldsymbol{G}_{\mathrm{rv}} \\ n\boldsymbol{G}_{\mathrm{vr}} & n^2\boldsymbol{G}_{\mathrm{vv}} \end{pmatrix}. \tag{30}$$

The singular value decomposition is performed as

$$\boldsymbol{G}^* = \boldsymbol{U\Sigma V}^T \tag{31}$$

where $\boldsymbol{\Sigma}$ = diag(Σ_1, Σ_2, ... , Σ_{n}) is a diagonal matrix of singular values and $\boldsymbol{U}$ and $\boldsymbol{V}$ are orthonormal matrices. The singular values in $\boldsymbol{\Sigma}$ in fact denote the gain of matrix $\boldsymbol{G}^*$ in various directions and are arranged in order of decreasing gain. Furthermore, the columns of the matrix $\boldsymbol{V}$ are eigenvectors of the matrix $\boldsymbol{G}^{*T}\boldsymbol{G}^*$. As column v_i corresponds to

Downloaded by TECHNISCHE UNIVERSITEIT DELFT on December 30, 2013 | http://arc.aiaa.org | DOI: 10.2514/6.2010-7885

Downloaded by TECHNISCHE UNIVERSITEIT DELFT on December 30, 2013 | http://arc.aiaa.org | DOI: 10.2514/6.2010-7885

singular value Σ_i, the eigenvector corresponding to the largest singular value is the direction with highest gain. In other words, eigenvector v_1 is the most observable 'direction' of the system and the largest value in that vector is the most observable state component. A further measure of observability that the SVD provides is the condition number κ of $\boldsymbol{\Sigma}$. The condition number is defined as the ratio of the largest and the smallest singular value in $\boldsymbol{\Sigma}$. A small value for κ indicates a good accuracy in the estimate (well-conditioned) whilst a large value for κ indicates poor accuracy (ill-conditioned). Since a small κ also indicates that all state components have comparable singular values, all state components will be well observable and thus can be estimated with good accuracy. If κ is larger, some state components have become less observable and can therefore not be estimated with the same accuracy as before.

Because an iterative batch LSQ algorithm is used, the observability of the system will change for each iteration since an updated reference state and an updated normal equations matrix are produced. The final result will therefore depend on the observability of the system in the last iteration and not of that in the first iteration. Thus, when the observability of the system is determined in the next section, this is done for the last iteration and not for the initial conditions.

Note that an alternative method to solve the issues with the units in the Gramian is provided by Ref. 16. There, the observability of the system is determined using the covariance matrix. In that case, the smallest singular value resulting from the SVD is the best observable state component. Normalization of the covariance matrix is performed in Ref. 16 by congruently transforming it using the square root of the information matrix:

$$\boldsymbol{P}^* = \sqrt{\boldsymbol{\Lambda}}\boldsymbol{P}\sqrt{\boldsymbol{\Lambda}}\ . \tag{32}$$

The singular values and eigenvectors are then calculated relative to the initial conditions of the system, provided that a priori information is used. This work however will use the Gramian to determine the observability of the system.

V. Simulation Results

A. Simulation setup

The absolute orbit of the chief spacecraft is assumed to be perfectly Keplerian with the following values for the absolute orbital elements at time t_0:

$$a = 7028\text{ km}\ ,\ e = 0\ ,\ i = 97.99^\circ\ ,\ \omega = 0^\circ\ ,\ \Omega = 0^\circ\ ,\ M_0 = 0^\circ\ .$$

Since we are interested in the observability of the system, the propagation of the orbits of the two satellites is performed using the CW equations. Thus, the dynamics in the estimator perfectly match the dynamics of the system under consideration. Out of a total of eight test cases considered for this study, the four most interesting ones are discussed here. These test cases are:

1a) 2D relative ellipse,
1b) 2D relative ellipse with drift in along-track direction,
2a) 3D safe ellipse,
2b) 3D safe ellipse with drift in along-track direction.

Case 1a is a closed-form periodic motion with a period of $2\pi/n$, which implies that the observability of the system does not increase for observation periods larger than one orbit. Case 1b however is not closed-form periodic, which should increase its observability over time. Contrary to case 1, the relative orbit in case 2 includes cross-track motion, which will affect the observability. Again due to the along-track drift, case 2b will be more observable than case 2a. The drift cases are all assumed to be due to a differential semi-major axis of 10 m. The true relative state components at t_0 for all cases are presented in Table 1. One hundred range measurements are performed per orbit for all cases. The number of orbits simulated is between 0.1 and 10 with steps of 0.1 orbits. For all four cases, a priori information is assumed to be available and can either be of poor or good quality. In case the a priori information is of poor quality, the initial state estimate is +100 m and +100n m/s off on all axes and the a priori variances are 100^2 m^2 for the positions and 100^2n^2 m^2/s^2 for the velocities. When good quality a priori information is available, the initial state estimate is +10 m and +10n m/s off on all axes and the a priori variances are 10^2 m^2 for the positions and 10^2n^2 m^2/s^2 for the velocities.

Downloaded by TECHNISCHE UNIVERSITEIT DELFT on December 30, 2013 | http://arc.aiaa.org | DOI: 10.2514/6.2010-7885

Table 1. Summary of test cases.

Case	Relative state elements at t_0 for Hill coordinates and for relative orbital elements											
	x_0 [m]	y_0 [m]	z_0 [m]	$\dot{x}_0$ [m/s]	$\dot{y}_0$ [m/s]	$\dot{z}_0$ [m/s]	$a\delta a$ [m]	$a\delta e_x$ [m]	$a\delta e_y$ [m]	$a\delta i_x$ [m]	$a\delta i_y$ [m]	$a\delta u$ [m]
1a	1000	0	0	0	-2.143	0	0	-1000	0	0	0	0
1b	1000	0	0	0	-2.149	0	-10	-1010	0	0	0	0
2a	1000	0	0	0	-2.143	-1.072	0	-1000	0	-1000	0	0
2b	1000	0	0	0	-2.149	-1.072	-10	-1010	0	-1000	0	0

B. Case 1: 2D Relative Ellipse

The relative orbits for this case are depicted in Fig. 2. The position of the chief is indicated by the red cross while the position of the deputy at time t_0 is indicated by a green circle. First, the results for the case without drift will be discussed, followed by a discussion of the results for the case with along-track drift.

1. 2D Relative Ellipse Without Drift (Case 1a)

Due to the use of range measurements only, multiple ambiguous solutions exist for this problem. These are four elliptical orbits ($a\delta i_x = \pm1732.1$ m and $a\delta u = \pm1000$ m) and two pendulum orbits ($a\delta e_x = \pm1000$ m), where a pendulum orbit is defined to be a relative orbit with cross-track motion but without along-track or radial motion. All these orbits will result in the same measurements and are thus equally valid solutions for the batch LSQ. Thus, if the initial state estimate is too far off the true state, the algorithm can converge to one of the ambiguous solutions, which is what happens in case only poor quality a priori information is available. Even the constraint imposed by $\Lambda\left(\boldsymbol{x}_0^{apr} - \boldsymbol{x}_0^{j}\right)$ cannot prevent this. For that to have any effect, the a priori covariances must be unrealistically small compared to the a priori state estimation error.

Between an observation arc length of 0.1 and 1 orbit, the error in the estimation of the relative orbit shows a somewhat erratic behavior. For these observation arc lengths, the Gramian is not always full rank and its condition number decreases from $1.1\cdot10^{16}$ at the start to $\sim1\cdot10^{5}$ at one orbit with a few large deviations from the general trend (i.e., a large increase in the condition number resulting in a decrease in matrix rank). This explains the erratic behavior for the state estimate between 0.1 and 1 orbit. For observation arc lengths longer than one orbit, the estimator always converges to a pendulum orbit with $a\delta u = -1000$ m and $a\delta i_x = 1732.1$ m. The other relative orbital elements are estimated to be zero The Gramian is always full rank and its condition number grows from ~7500 at one orbit to $\sim4.4\cdot10^{5}$ at ten orbits, which implies that this problem is locally observable and well conditioned during that period but that the observability deteriorates for longer measurement arcs.

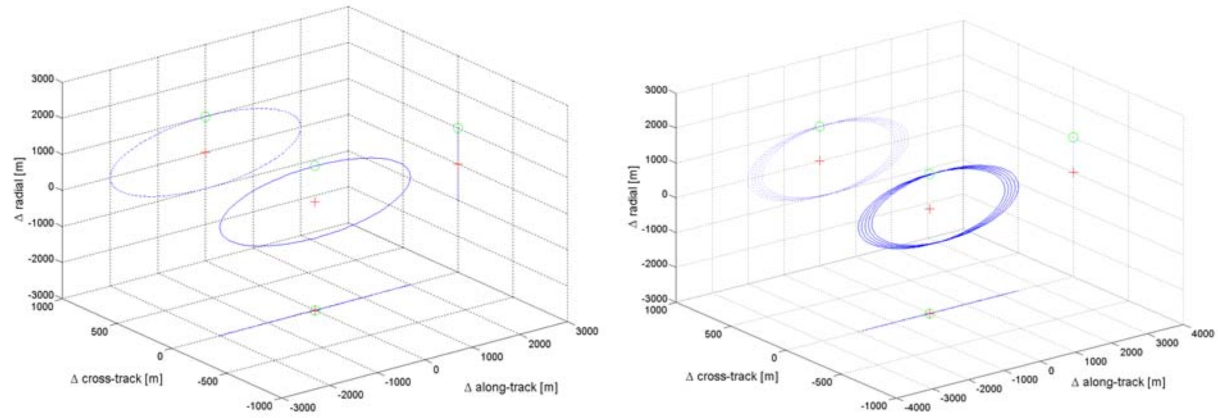

(a) (b)

Figure 2. 2D relative ellipse without (a) and with (b) along-track drift. The position of the chief is indicated by the red cross while the position of the deputy at time t_0 is indicated by a green circle.

Downloaded by TECHNISCHE UNIVERSITEIT DELFT on December 30, 2013 | http://arc.aiaa.org | DOI: 10.2514/6.2010-7885

Table 2. Estimation errors and standard deviations for an observation arc length of 10 orbits for case 1a using good quality and 'proper' a priori information.

	x_0	y_0	z_0	$\dot{x}_0$	$\dot{y}_0$	$\dot{z}_0$	$a\delta a$	$a\delta e_x$	$a\delta e_y$	$a\delta i_x$	$a\delta i_y$	$a\delta u$
	[m]	[m]	[m]	[mm/s]	[mm/s]	[mm/s]	[m]	[m]	[m]	[m]	[m]	[m]
Estimation error	0.02	-0.06	-7.80	-0.03	-0.04	-11.48	~0	-0.02	0.03	-10.71	7.80	1.09
Standard deviation	0.03	0.14	7.18	0.06	0.07	10.41	~0	0.03	0.06	9.71	7.18	1.01

For the case where good quality a priori information available, it can be argued that it is not unrealistic to assume that we also know the type of relative orbit (e.g., along-track, pendulum, ellipse) the satellites are in. Given that this case is a closed-form periodic solution of the CW equations, the relationships $\dot{y}_0 = -2nx_0$ and $y_0 = 2\dot{x}_0/n$ hold. Therefore, $\dot{y}_0^{apr} \approx -2nx_0^{apr}$ and $y_0^{apr} \approx 2\dot{x}_0^{apr}/n$ must hold as well. Thus, for this case, a 'proper' a priori relative state estimate requires that $\dot{y}_0^{apr} \approx -2200n$ and $\dot{x}_0^{apr} \approx 50n$. With 'proper' a priori conditions in place, the only incorrect solution the estimator can converge to is the incorrect ambiguous solution on the same relative orbit, which will occur if the a priori estimate is closer to this solution than to the correct solution.

When good quality and 'proper' a priori dynamics are applied, the estimator is able to improve upon the a priori estimate for all observation arc lengths and converges to the correct state estimate. However, this is completely due to the use of the information matrix $\boldsymbol{\Lambda}$ in the estimator since now the rank of the Gramian is almost always five, indicating a locally non-observable system. Since the relative motion repeats after one orbit, no new information regarding the dynamics is added, which results in similar estimation accuracies for all observation arcs longer than one orbit. As shown in Table 2, the estimation errors and standard deviations of the estimate stabilize at relatively large values for the out-of-plane components for observation arc lengths longer than one orbit. The reason for this is as follows. For an observation arc length of ten orbits, the singular values are

$$\Sigma_1 = 4.0\times10^7,\ \Sigma_2 = 1.3\times10^3,\ \Sigma_3 = 4.9\times10^2,\ \Sigma_4 = 6.6\times10^1,\ \Sigma_5 = 1.2\times10^{-2},\ \Sigma_6 = 5.0\times10^{-14}.$$

The very small value for Σ_6 indicates that the state represented by eigenvector v_6 is the least observable state and is unobservable in practice. The corresponding eigenvector matrices for Hill coordinates ($\boldsymbol{V_x}$) and for relative orbital elements ($\boldsymbol{V_{\delta\alpha}}$) are

$$\boldsymbol{V}_x = \left(\begin{pmatrix}-0.89\\0.00\\0.00\\-0.01\\-0.45\\0.00\end{pmatrix}\begin{pmatrix}0.04\\-0.29\\0.00\\0.95\\-0.09\\0.00\end{pmatrix}\begin{pmatrix}-0.45\\0.00\\0.00\\0.10\\0.89\\0.00\end{pmatrix}\begin{pmatrix}-0.02\\-0.96\\0.01\\-0.29\\0.03\\0.01\end{pmatrix}\begin{pmatrix}0.00\\0.00\\-0.95\\0.00\\0.00\\0.32\end{pmatrix}\begin{pmatrix}0.00\\-0.01\\-0.32\\0.00\\0.00\\-0.95\end{pmatrix}\right), \quad \boldsymbol{V}_{\delta\alpha} = \left(\begin{pmatrix}-1.00\\0.00\\0.00\\0.00\\0.00\\0.02\end{pmatrix}\begin{pmatrix}0.00\\-1.00\\0.00\\0.00\\0.00\\-0.02\end{pmatrix}\begin{pmatrix}0.00\\0.00\\-1.00\\0.00\\0.00\\0.00\end{pmatrix}\begin{pmatrix}0.02\\-0.02\\0.00\\0.00\\-0.14\\0.99\end{pmatrix}\begin{pmatrix}0.00\\0.00\\0.00\\-0.33\\-0.94\\-0.13\end{pmatrix}\begin{pmatrix}0.00\\0.00\\0.00\\-0.95\\0.32\\0.05\end{pmatrix}\right).$$

It is known[16] that large differences between singular values, such as between Σ_1 and Σ_2, are an indication for the existence of a special linear combination of state components. When inspecting the eigenvectors of the SVD, we see that this is indeed the case: The most observable eigenvector in Hill coordinates is a clear hint at the well known relationship[11] $\Delta a = 4x_0 + 2\dot{y}_0/n$. Thus, it can be expected that the most observable state for the relative orbital elements is the relative semi-major axis. And indeed, $\boldsymbol{V_{\delta\alpha}}$ shows that this is true. Furthermore, the results for the eigenvector matrices agree with intuition in that the most observable state components are the in-plane components while the least observable state components are the out-of-plane components. Due to the fact that there is no out-of-plane motion and that the out-of-plane state components are the least observable states, it is not surprising that these states are poorly estimated. Figure 3 depicts how the eigenvectors of the SVD evolve over time for the relative orbital elements. Stabilization occurs after roughly one orbit, which agrees with the observation that no new information is added after that period. Note that Fig. 3 shows the absolute values of the elements of the eigenvectors.

Note that for different initial relative states, the observability of the various state components changes. For instance, δe_y becomes more observable than δe_x and δi_x becomes more observable than δi_y in case $x_0 = 0$. In addition, the direction of all eigenvectors changes for different initial relative states, except for v_1, which always stays the same. Thus, the linear combination between x_0 and $\dot{y}_0$ is always preserved while other seemingly present linear

Downloaded by TECHNISCHE UNIVERSITEIT DELFT on December 30, 2013 | http://arc.aiaa.org | DOI: 10.2514/6.2010-7885

combinations (like e.g. between z_0 and $\dot{z}_0$ in eigenvectors v_5 and v_6) vanish. For this subcase, the differential semi-major axis is always the most observable state component, followed by the other in-plane state components (δe_x, δe_y, and δu), which are in turn followed by the out-of-plane state components (δi_x and δi_y).

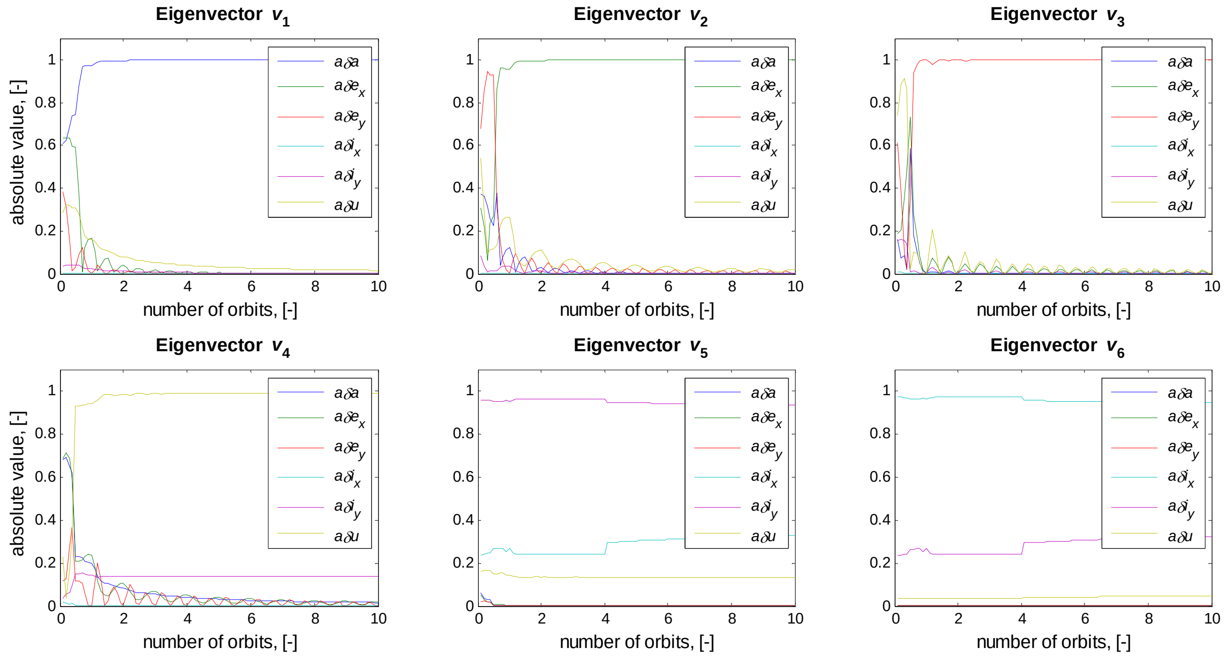

Figure 3. Evolution over time of the observability eigenvectors for the relative orbital elements for case 1a when using a good quality and 'proper' a priori state estimate. The values for the elements of the eigenvectors are shown in absolute values.

2. *2D Ellipse With Drift in Along-Track Direction (Case 1b)*

Using a good quality and 'proper' a priori state estimate results in a correct estimate for the relative state for all observation arc lengths. For almost all observation arc lengths the Gramian is full rank and $\kappa \approx 10^{10}$, indicating an observable but not very well conditioned system. Due to the extra information caused by the along-track drift, the estimation for this case is slightly better than for case 1a, cf. Table 3. The singular values and the corresponding observability eigenvectors for an observation arc length of ten orbits are now

$$\Sigma_1 = 4.1\times10^7,\ \Sigma_2 = 1.4\times10^3,\ \Sigma_3 = 4.6\times10^2,\ \Sigma_4 = 7.4\times10^1,\ \Sigma_5 = 1.0\times10^{-2},\ \Sigma_6 = 2.1\times10^{-3}$$

$$\boldsymbol{V}_x = \left(\begin{pmatrix} -0.89 \\ 0.00 \\ 0.00 \\ -0.01 \\ -0.45 \\ 0.00 \end{pmatrix} \begin{pmatrix} -0.03 \\ 0.27 \\ 0.00 \\ -0.96 \\ 0.07 \\ 0.00 \end{pmatrix} \begin{pmatrix} 0.45 \\ -0.02 \\ 0.00 \\ -0.08 \\ -0.89 \\ -0.00 \end{pmatrix} \begin{pmatrix} -0.02 \\ -0.96 \\ 0.00 \\ -0.27 \\ 0.03 \\ 0.00 \end{pmatrix} \begin{pmatrix} 0.00 \\ 0.00 \\ -1.00 \\ 0.00 \\ 0.00 \\ 0.00 \end{pmatrix} \begin{pmatrix} 0.00 \\ 0.00 \\ 0.00 \\ 0.00 \\ 0.00 \\ 1.00 \end{pmatrix} \right), \quad \boldsymbol{V}_{\delta\alpha} = \left(\begin{pmatrix} -1.00 \\ -0.01 \\ 0.00 \\ 0.00 \\ 0.00 \\ 0.02 \end{pmatrix} \begin{pmatrix} 0.01 \\ -1.00 \\ 0.01 \\ 0.00 \\ 0.00 \\ -0.02 \end{pmatrix} \begin{pmatrix} 0.00 \\ 0.01 \\ -1.00 \\ 0.00 \\ 0.00 \\ 0.00 \end{pmatrix} \begin{pmatrix} -0.02 \\ 0.02 \\ 0.00 \\ 0.00 \\ 0.14 \\ -0.99 \end{pmatrix} \begin{pmatrix} 0.00 \\ 0.00 \\ 0.00 \\ 0.00 \\ -0.99 \\ -0.14 \end{pmatrix} \begin{pmatrix} 0.00 \\ 0.00 \\ 0.00 \\ -1.00 \\ 0.00 \\ 0.00 \end{pmatrix} \right).$$

We again see similar relations between the different eigenvectors as in case 1a. In addition, just as for case 1a, when we choose initial conditions such that x_0 is close to 0, δi_x is more observable than δi_y and δe_y is more observable than δe_x.

Since the along-track drift provides extra information, it is interesting to investigate whether after a certain observation arc length a correct estimate for the initial relative state can be obtained even with poor quality a priori information. Running the estimator as such leads to the following. For observation arc lengths less than one orbit, the behavior of the estimate is erratic and can be very far off from the correct solution, which is caused by a lack of observation data. For observation arc lengths of one up to roughly six orbits, the relative orbit is estimated to be a pendulum orbit. This estimate quite suddenly changes to the ambiguous solution on the correct elliptical relative orbit for observation arc lengths of roughly six orbits or more, cf. Fig. 4. Unfortunately, convergence to the incorrect

Downloaded by TECHNISCHE UNIVERSITEIT DELFT on December 30, 2013 | http://arc.aiaa.org | DOI: 10.2514/6.2010-7885

ambiguous initial relative state cannot be prevented in this setting since a rigid body rotation of the formation from the correct initial relative state to the incorrect ambiguous initial relative state cannot be distinguished using range measurements alone. It depends entirely on the initial estimate whether or not the solution converges to the ambiguous solution or not. Notice in Fig. 4 that the change in the estimation occurs when the estimate for the relative semi-major axis is close to its true magnitude (but with wrong sign). Once the estimator has converged to the correct relative orbit, the standard deviations in the solution are similar to those shown earlier for this case with the standard deviations of the out-of-plane state components much worse than those of the in-plane state components.

The change in observability after six orbits is also very well visualized in the observability eigenvectors, cf. Fig. 5. Notice from Fig. 5 that the observability of the relative semi-major axis stays constant with time and that δu is the least observable state component up to roughly six orbits, which explains why the estimator converges to a pendulum orbit up to this time (and why it also did that for case 1a with poor a priori information). The change in observability of the various states is accompanied by a jump in the condition number of $2\cdot10^5$ to $\sim10^8$. If we now increase the error in the a priori estimation by one order of magnitude, the estimator requires an observation arc length of roughly 8.2 orbits before it converges to the incorrect ambiguous initial relative state. When we change the sign of the estimation errors, the estimator converges to the correct initial relative state after roughly 3.3 orbits. Changing the differential semi-major axis to 100 m to increase the drift rate leads to an incorrect ambiguous initial relative state estimate after roughly 1.5 orbits. Increasing the number of observations per unit of time has no effect on the observation arc length needed to arrive at the correct ambiguous solution. Thus, the magnitude and sign of the initial estimation errors as well as the relative drift rate have a large impact on the observation arc length needed before the estimator converges to the correct solution.

Table 3. Estimation errors and standard deviations for an observation arc length of 10 orbits for case 1b using good quality and 'proper' a priori information.

	x_0 [m]	y_0 [m]	z_0 [m]	$\dot{x}_0$ [mm/s]	$\dot{y}_0$ [mm/s]	$\dot{z}_0$ [mm/s]	$a\delta a$ [m]	$a\delta e_x$ [m]	$a\delta e_y$ [m]	$a\delta i_x$ [m]	$a\delta i_y$ [m]	$a\delta u$ [m]
Estimation error	0.01	-0.03	-6.65	-0.01	-0.03	-9.61	~0	-0.01	0.01	-8.97	6.65	0.93
Standard deviation	0.03	0.12	7.04	0.05	0.06	9.73	~0	0.03	0.04	9.08	7.04	0.99

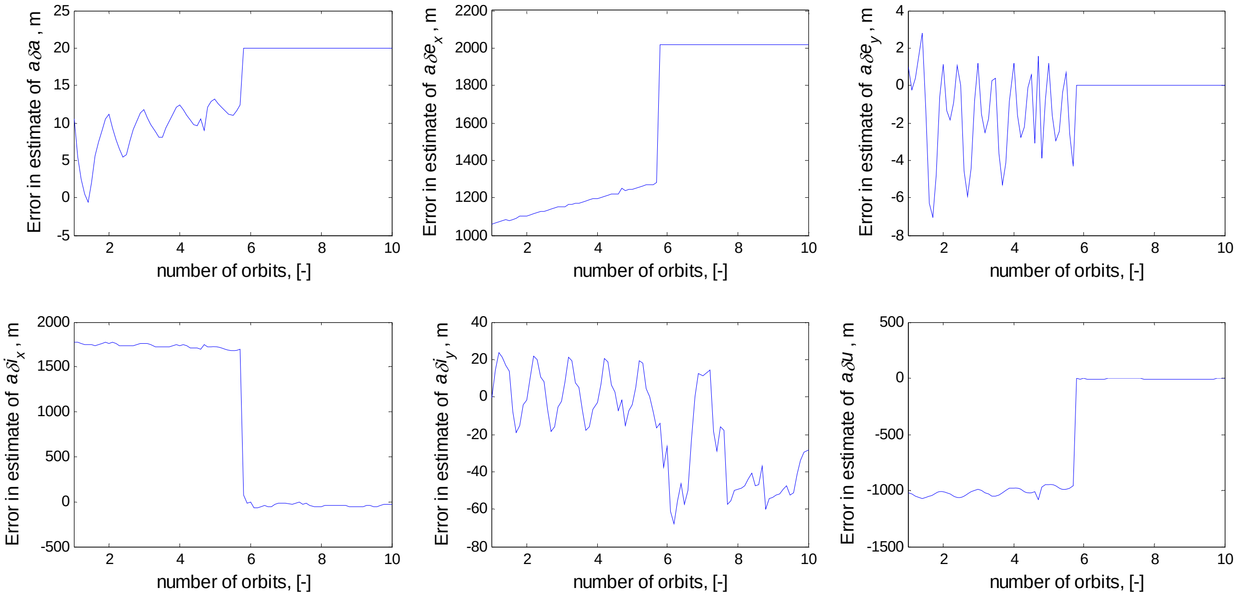

Figure 4. Evolution over time of the errors in the estimation of the relative orbital elements for case 1b with poor quality a priori information.

Downloaded by TECHNISCHE UNIVERSITEIT DELFT on December 30, 2013 | http://arc.aiaa.org | DOI: 10.2514/6.2010-7885

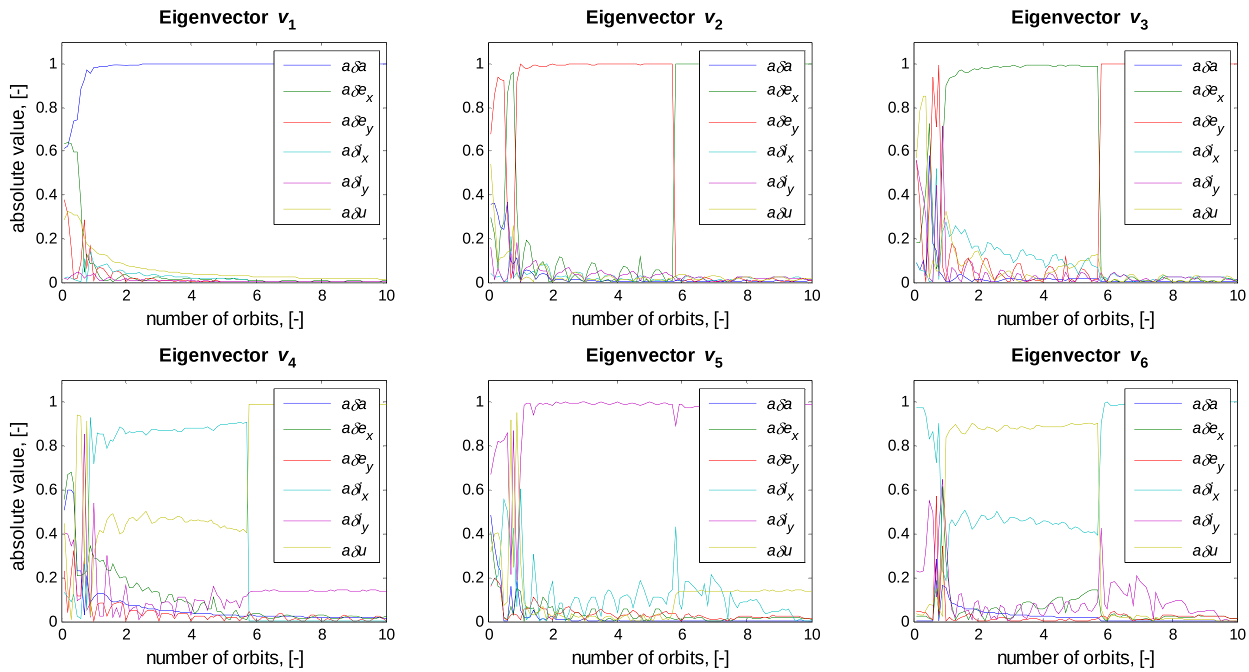

Figure 5. Evolution over time of the observability eigenvectors for the relative orbital elements for case 1b with poor quality a priori information. The elements of the eigenvectors are shown in absolute values.

C. Case 2: 3D Safe Ellipse

Compared to case 1, this case is more complex due to the existence of cross-track components in the relative motion. This has profound effects for both cases considered. The relative orbits for this case are depicted in Fig. 6.

1. 3D Safe Ellipse Without Drift (Case 2a)

In case of poor quality a priori information, the result obtained for this case is similar to the result obtained in case 1a: The rank of the Gramian is always six and the condition number for observation arcs longer than 1 orbit grows from ~7500 at ~1 orbit to $4.4\cdot10^5$ at 10 orbits, indicating a well-conditioned system for which the observability is very comparable to that of case 1a. For observation arcs longer than 1 orbit, the least observable state component is δu and the estimator always converges to a pendulum orbit.

In case of a good quality and 'proper' a priori state estimate, the estimator converges to the correct relative orbit for all observation arc lengths. However, this case differs from case 1a in that now the out-of-plane state components do not necessarily have the largest errors and standard deviations, cf. Table 4, which is caused by the existence of out-of-plane relative motion. The singular values and corresponding observability eigenvectors for an observation arc of 10 orbits are:

$$\Sigma_1 = 3.3\times10^7,\ \Sigma_2 = 1.1\times10^3,\ \Sigma_3 = 4.9\times10^2,\ \Sigma_4 = 8.5\times10^1,\ \Sigma_5 = 8.6\times10^0,\ \Sigma_6 = 2.3\times10^{-11}$$

$$\boldsymbol{V}_x = \left(\begin{pmatrix}-0.89\\0.00\\0.00\\-0.01\\-0.45\\0.00\end{pmatrix}\begin{pmatrix}0.04\\-0.28\\0.13\\0.94\\-0.10\\-0.05\end{pmatrix}\begin{pmatrix}0.41\\0.00\\-0.04\\-0.12\\-0.81\\-0.40\end{pmatrix}\begin{pmatrix}0.02\\0.80\\0.58\\0.15\\-0.03\\-0.02\end{pmatrix}\begin{pmatrix}-0.18\\0.00\\0.00\\0.00\\0.36\\-0.91\end{pmatrix}\begin{pmatrix}0.00\\0.53\\-0.80\\0.27\\0.00\\0.00\end{pmatrix}\right),\quad \boldsymbol{V}_{\delta\alpha} = \left(\begin{pmatrix}-1.00\\0.00\\0.00\\0.00\\0.00\\0.02\end{pmatrix}\begin{pmatrix}0.00\\-0.98\\0.00\\-0.19\\0.00\\-0.02\end{pmatrix}\begin{pmatrix}0.00\\0.00\\0.95\\0.00\\0.32\\-0.02\end{pmatrix}\begin{pmatrix}0.02\\-0.02\\0.06\\0.00\\-0.12\\0.99\end{pmatrix}\begin{pmatrix}0.00\\-0.19\\0.00\\0.98\\0.00\\0.00\end{pmatrix}\begin{pmatrix}0.00\\0.00\\0.31\\-0.01\\-0.94\\-0.13\end{pmatrix}\right).$$

Just as for case 1a, the rank of the Gramian is almost always five, indicating a locally non-observable system. It is noted that the chosen initial relative state for this case is a limit case for which δa, δe_x and δi_x can be estimated relatively well. For all other initial states where $x_0 \neq 0$, the standard deviation in the estimation of these state components is larger. However, the relative semi-major axis is always the most observable state component and its

Downloaded by TECHNISCHE UNIVERSITEIT DELFT on December 30, 2013 | http://arc.aiaa.org | DOI: 10.2514/6.2010-7885

estimation strongly improves with time. For an observation arc length of more than 1 orbit, the results for the other relative orbital elements either do not improve with time or improve much less fast.

Table 4. Estimation errors and standard deviations for an observation arc length of 10 orbits for case 2a using good quality and 'proper' a priori information.

	x_0	y_0	z_0	$\dot{x}_0$	$\dot{y}_0$	$\dot{z}_0$	$a\delta a$	$a\delta e_x$	$a\delta e_y$	$a\delta i_x$	$a\delta i_y$	$a\delta u$
	[m]	[m]	[m]	[mm/s]	[mm/s]	[mm/s]	[m]	[m]	[m]	[m]	[m]	[m]
Estimation error	~0	0.66	-0.99	0.35	0.01	-0.02	~0	~0	-0.33	-0.02	0.99	0.14
Standard deviation	0.07	5.34	8.02	2.86	0.14	0.34	~0	0.07	2.67	0.32	8.02	1.13

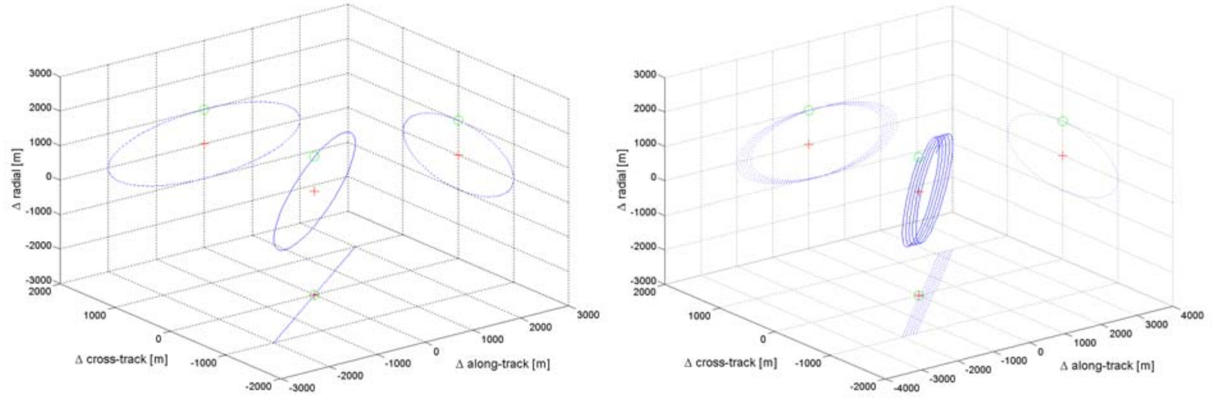

(a) (b)

Figure 6. 3D safe ellipse without (a) and with (b) along-track drift.

2. 3D Safe Ellipse With Drift in Along-Track Direction (Case 2b)

When using good quality and 'proper' a priori information, the rank of the Gramian is always six and the condition number varies between $1 \cdot 10^6$ at ~1 orbit to $5.5 \cdot 10^6$ after 10 orbits, which indicates a well-conditioned system. In fact, the observability of this case is orders of magnitude better than case 1b. This is reflected in the result for the state estimation, cf. Table 6, which is much better than for case 1b. This result is also clearly expressed in the singular values, where the difference between Σ_2 and Σ_6 is only three orders of magnitude, and the corresponding observability eigenvectors:

$$\Sigma_1 = 3.4 \times 10^7,\ \Sigma_2 = 1.2 \times 10^3,\ \Sigma_3 = 4.5 \times 10^2,\ \Sigma_4 = 8.4 \times 10^1,\ \Sigma_5 = 2.1 \times 10^1,\ \Sigma_6 = 6.2 \times 10^0$$

$$\boldsymbol{V}_x = \left(\begin{pmatrix} -0.89 \\ 0.00 \\ 0.00 \\ -0.01 \\ -0.45 \\ 0.00 \end{pmatrix} \begin{pmatrix} 0.02 \\ -0.26 \\ 0.10 \\ 0.96 \\ -0.06 \\ -0.04 \end{pmatrix} \begin{pmatrix} 0.40 \\ -0.02 \\ -0.03 \\ -0.08 \\ -0.79 \\ -0.46 \end{pmatrix} \begin{pmatrix} 0.02 \\ 0.82 \\ 0.54 \\ 0.16 \\ -0.03 \\ -0.02 \end{pmatrix} \begin{pmatrix} -0.01 \\ -0.51 \\ 0.83 \\ -0.22 \\ 0.01 \\ -0.01 \end{pmatrix} \begin{pmatrix} -0.21 \\ 0.01 \\ -0.01 \\ 0.00 \\ 0.41 \\ -0.89 \end{pmatrix} \right), \quad \boldsymbol{V}_{\delta\alpha} = \left(\begin{pmatrix} -1.00 \\ -0.01 \\ 0.00 \\ 0.00 \\ 0.00 \\ 0.02 \end{pmatrix} \begin{pmatrix} 0.01 \\ -0.98 \\ 0.01 \\ -0.22 \\ 0.00 \\ -0.02 \end{pmatrix} \begin{pmatrix} 0.00 \\ -0.01 \\ -0.98 \\ 0.00 \\ -0.21 \\ 0.01 \end{pmatrix} \begin{pmatrix} -0.02 \\ 0.02 \\ -0.05 \\ 0.00 \\ 0.15 \\ -0.99 \end{pmatrix} \begin{pmatrix} 0.00 \\ 0.00 \\ 0.21 \\ -0.01 \\ -0.96 \\ -0.16 \end{pmatrix} \begin{pmatrix} 0.00 \\ 0.22 \\ 0.00 \\ -0.98 \\ 0.01 \\ 0.01 \end{pmatrix} \right).$$

It is noted that for this case, between ~1 and ~5.5 orbits, δi_x is more observable than δi_y. For longer observation arc lengths, δi_y is more observable than δi_x. This change in observability does not happen for case 1b with good quality and 'proper' a priori information.

When now using poor quality a priori information, the result is an incorrect ambiguous relative initial state estimate after an observation arc length of 8.5 orbits or more, cf. Fig. 7. Between 1 and 8.5 orbits, the estimated relative orbit is a pendulum orbit, which is again caused by δu being the least observable state component up to then. Again, the observation arc length required before the estimator converges to the correct relative orbit depends on the drift rate and the error in the initial relative state estimate. Note that the change in observability now occurs later

Downloaded by TECHNISCHE UNIVERSITEIT DELFT on December 30, 2013 | http://arc.aiaa.org | DOI: 10.2514/6.2010-7885

than for case 1b and that the condition number now jumps from $6.5{\cdot}10^5$ to only $4{\cdot}10^6$, indicating a much better observable system after the change in observability than for case 1b.

Table 6. Estimation errors and standard deviations for an observation arc length of 10 orbits for case 2b using good quality and 'proper' a priori information.

	x_0 [m]	y_0 [m]	z_0 [m]	$\dot{x}_0$ [mm/s]	$\dot{y}_0$ [mm/s]	$\dot{z}_0$ [mm/s]	$a\delta a$ [m]	$a\delta e_x$ [m]	$a\delta e_y$ [m]	$a\delta i_x$ [m]	$a\delta i_y$ [m]	$a\delta u$ [m]
Estimation error	-0.01	~0	~0	~0	0.01	-0.03	~0	0.01	~0	-0.02	~0	~0
Standard deviation	0.08	0.14	0.19	0.06	0.18	0.38	~0	0.08	0.06	0.36	0.19	0.09

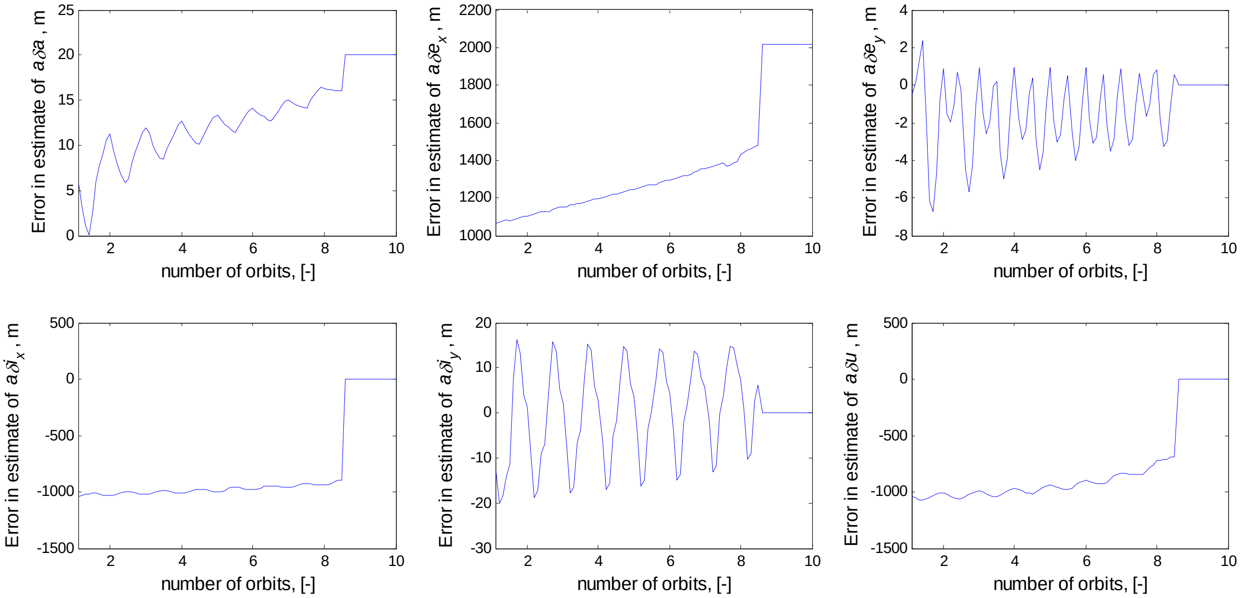

Figure 7. Evolution over time of the errors in the estimation of the relative orbital elements for case 2b with poor quality a priori information.

D. Note on the Estimation Accuracy of the Semi-Major Axis

For all cases treated in this paper, it has been observed that the differential semi-major axis can always be estimated with almost perfect accuracy. As is shown in Refs. 17-19, this is not a coincidence since for near-circular orbits, the accuracy of the estimation of the relative semi-major axis is given by Refs. 17-19 as

$$\sigma_{\delta a} = 2\sqrt{4\sigma_x^2 + \frac{4}{n}\rho_{x\dot{y}}\sigma_x\sigma_{\dot{y}} + \frac{1}{n^2}\sigma_{\dot{y}}^2} \tag{33}$$

where $\rho_{x\dot{y}}$ is the correlation between the state components x and $\dot{y}$ and is defined as

$$\rho_{x\dot{y}} = \frac{\rho_{x\dot{y}}\sigma_x\sigma_{\dot{y}}}{\sigma_x\sigma_{\dot{y}}} = \frac{\mathrm{Cov}(x,\dot{y})}{\sqrt{\mathrm{Cov}(x,x)}\sqrt{\mathrm{Cov}(\dot{y},\dot{y})}}\,. \tag{34}$$

For the conditions $\rho_{x\dot{y}} = -1$ and $\sigma_{\dot{y}}/\sigma_x = 2n$, which are called the correlation and balance conditions respectively, the result for Eq. (33) is $\sigma_{\delta a} = 0$. As $n = 1.08{\cdot}10^{-3}$ rad/s, it is easy to verify with the results provided in subsections V.A and V.B that the balance condition indeed approximately holds for the cases shown. In addition,

Downloaded by TECHNISCHE UNIVERSITEIT DELFT on December 30, 2013 | http://arc.aiaa.org | DOI: 10.2514/6.2010-7885

although not shown in the paper, the correlation between x and $\dot{y}$ is also always very close to -1 for the cases considered and thus both conditions hold, leading to an almost perfect estimate for the differential semi-major axis. However, as is proven in Ref. 18, a perfect estimate for the relative semi-major axis is not achievable in practice. The reason for this is that in practice, a sequential estimator, e.g. an extended Kalman filter (EKF), will be used. According to Ref. 18, the earlier mentioned correlation and balance conditions are intrinsically incompatible for an EKF and can therefore never be achieved simultaneously. With current dynamic models and using carrier-phase differential GPS (CDGPS) to estimate relative positions, Ref. 18 reports that typical correlations observed in practice are ≈ -0.1, which is far off the desired value of -1. Since the estimator used in this analysis does not suffer from process noise and since in this analysis the dynamic model is perfect, the correlation and balance requirements can be met.

VI. Conclusions & Future Work

In this paper, an analysis has been performed on the observability of the relative orbital elements for two satellites flying in formation in a low Earth orbit. Information on the change in relative state with time was provided by inter-satellite range measurements only which were processed in a batch least-squares algorithm together with a perfect dynamic model in order to estimate the initial relative state. The observability of the various relative orbital elements was analyzed using a singular value decomposition of the Gramian matrix. Several test cases with 2D and 3D relative elliptical motion and with and without drift in along-track direction were analyzed.

For observation arc lengths less than one orbit, the observability of the system generally improves for increasing observation arc length due to the addition of new information on the system dynamics. To achieve a correct initial relative state estimate in this phase, it is vital to have good quality a priori information. In case of poor quality a priori information, the behavior of the solution is very erratic due to the continuously changing observability for the different relative orbital elements.

No along-track drift and observation arc lengths larger than one orbit lead to the following. For good quality and ‘proper’ a priori information (‘proper’ here means a correct initial estimate of the type of relative orbit), the actual system itself becomes locally unobservable. Yet, due to the use of the information matrix in the estimator, a solution can be obtained that is close to the true initial relative state. When only in-plane motion is present, the estimation of the out-of-plane states is relatively poor due to them being the least observable states and due to the in-plane motion only. When out-of-plane motion is also present, the out-of-plane states are still the least observable states, but they are not necessarily the states for which the estimation errors and standard deviations are the largest. Starting with poor quality a priori information leads to a locally observable and well-conditioned system with a condition number on the order of 10^3 to 10^5, but the estimated relative orbit is a pendulum orbit (a relative orbit without a differential semi-major axis but with a relative inclination) due to the relative mean argument of latitude δu being the least observable state component. Surprisingly, there is no apparent difference in observability between the in-plane and out-of-plane case here.

The inclusion of along-track drift has profound implications for observation arc lengths longer than one orbit. In case of good quality and ‘proper’ a priori information, the system is now locally observable. For in-plane motion only however, the condition number of the system is rather high (order 10^{10}), leading to an only slightly better state estimate than in case of a closed-form periodic relative orbit. When out-of-plane motion is added, the drift leads to a significantly better estimate than for the no drift case, which is caused by the system now having a much lower condition number (order 10^6). Especially the estimation of the out-of-plane states improves significantly here. For the case of poor quality a priori information, the extra information resulting from the along-track drift allows the estimator to converge to the correct relative orbit after sufficient information has been gathered, which is not possible when drift is absent. However, due to ambiguity, convergence to the correct initial relative state cannot be guaranteed. The point in time where the change in observability occurs depends on the type of relative orbit (2D or 3D), the magnitude and sign of the initial estimate and on the drift rate. The number of observations has no influence on this. For the 3D case, the observability of the system after the change in observability, which then becomes of order 10^6, is better than for the 2D case, which becomes of order 10^8.

The observability of the system in the cases with drift is of practical interest since in reality a drift-free relative motion is impossible to achieve. Thus, provided that the satellites are allowed to drift for a sufficiently long amount of time, the system will always be observable, even though it can take a long time before the estimator converges to the correct relative orbit. However, as already stated, in case of poor quality a priori information the estimator can converge to an incorrect solution due to ambiguity. If no other means are available, this ambiguity can only be resolved using a small maneuver in a known direction. Once the ambiguity has been resolved, the satellites can be guided and controlled into a non-drifting relative state which, due to the information gained in the drifting state, can

Downloaded by TECHNISCHE UNIVERSITEIT DELFT on December 30, 2013 | http://arc.aiaa.org | DOI: 10.2514/6.2010-7885

be estimated with good accuracy. The relative semi-major axis is always the most observable state, followed by the relative eccentricity vector components. The relative mean argument of latitude and the relative inclination vector components are always the least observable states.

Future work on this topic will concentrate on the incorporation of the J_2 perturbation into the dynamic model, which is expected to increase the observability of the system in case of absolute orbit propagation using more realistic gravity fields. Furthermore, a comparison will be made between the observability of the relative orbital elements obtainable with noisy inter-satellite range measurements only and with a combination of noisy inter-satellite range measurements and noisy relative line-of-sight measurements. The latter measurements will be constructed from inter-satellite range measurements obtained with multiple antennas on the same satellite. This comparison will allow the identification of those cases where the combination of inter-satellite range, range measurement error, and antenna baseline is such that the additional noisy relative line-of-sight measurements do not substantially increase the observability of the system. This is of both practical and academic interest since for those cases, a relatively simple system with inter-satellite range measurements only would perform just as well as a more complex system with added relative line-of-sight measurements.

References

[1] D'Amico, S. and Montenbruck, O., "Proximity Operations of Formation-Flying Spacecraft Using an Eccentricity/Inclination Vector Separation," *Journal of Guidance, Control & Dynamics*, Vol. 29, No. 3, 2006, pp. 554-563.

[2] Markley, F., "Autonomous Navigation Using Landmark and Inter-Satellite Data," *Proceedings of the AIAA/AAS Astrodynamics Conference*, Seattle, WA, USA, Aug. 20-22, 1984.

[3] Psiaki, M., "Autonomous Orbit Determination for Two Spacecraft from Relative Position Measurements," *Journal of Guidance, Control & Dynamics*, Vol. 22, No. 2, 1999, pp. 305-312.

[4] Yim, J., Crassidis, J., Junkins, J., "Autonomous orbit determination of two spacecraft system using relative line of sight vector measurements," *Proceedings of the AAS/AIAA Spaceflight Mechanics Meeting*, Maui, HI, USA, AAS paper 04-257, 2004.

[5] Doolittle, C., Chavez, F., Lovell, T., "Relative Orbit Element Estimation for Satellite Navigation," *Proceedings of AIAA Guidance, Navigation, and Control Conference and Exhibit*, San Francisco, CA, USA, Aug. 15-18, 2005.

[6] Woffinden, D. and Geller, D., "Relative Angles-Only Navigation and Pose Estimation for Autonomous Orbital Rendezvous," *Journal of Guidance, Control & Dynamics*, Vol. 30, No. 5, 2007, pp. 1455–1469.

[7] Woffinden, D. and Geller, D., "Observability Criteria for Angles-Only Navigation," *IEEE Trans. On Aerosp. And Elec. Syst.*, Vol. 45, No. 3, 2009, pp.1194-1208.

[8] Kang, W., Ross, M., Pham, K., Gong, Q., "Autonomous Observability of Networked Multisatellite Systems," *Journal of Guidance, Control & Dynamics*, Vol. 32, No. 3, 2009, pp. 869-877.

[9] Chavez, F. and Lovell, T., "Relative-Orbit Element Estimation for Satellite Navigation and Guidance," *Proceedings of the AIAA/AAS Astrodynamics Specialist Conference and Exhibit*, Providence, RI, USA, Aug. 16-19, 2004.

[10] Hill, G.W., "Researches in the Lunar Theory," *American journal of Mathematics*, Vol. 1, 1878, pp. 5-26.

[11] Montenbruck, O. and Gill, E., "Satellite Orbits – Models, Methods, Applications," 1st ed., 3rd printing, Springer-Verlag Berlin Heidelberg, 2005, ISBN 978-3-540-67280-7.

[12] D'Amico, S., De Florio, S., Larsson, R., Nylund, M., "Autonomous formation keeping and reconfiguration for remote sensing spacecraft," *Proceedings of the 21st International Symposium on Space Flight Dynamics*, Toulouse, France, Sept. 28 – Oct. 2, 2009.

[13] Gill, E., D'Amico, S., Montenbruck, O., "Autonomous Formation Flying fort he PRISMA Mission," *Journal of Guidance, Control & Dynamics*, Vol. 44, No. 3, 2007, pp. 671-681.

[14] Cai, Z., Zhao, D., Chen, J., Jiao, W., "Research on Autonomous Orbit Determination of Navigation Satellite Based on Crosslink Range and Orientation Parameters Constraining," *Journal of Geo-Spatial Information Science*, Vol. 9, No. 1, March 2006, pp.18-23.

[15] Huxel, P., "Navigation Algorithms and Observability Analysis for Formation Flying Missions," Ph.D. dissertation, University of Texas at Austin, Austin, TX, USA, 2006.

[16] Ham, F. and Brown, R., "Observability, Eigenvalues, and Kalman Filtering," *IEEE Trans. On Aerosp. And Elec. Syst.*, Vol. AES-19, No. 2, March 1983, pp. 269-273.

[17] Carpenter, J. and Alfried, K., "Navigation Accuracy Guidelines for Orbital Formation Flying," *Journal of the Astronautical Sciences*, Vol. 53, No. 2, 2005, pp. 207-219.

[18] How, J.P., Alfried, K.T., Breger, L., Mitchell, M., "Semimajor Axis Estimation Strategies," *Proceedings of the 2nd International Symposium on Formation Flying Missions and Technologies*, Washington DC, USA, Sept. 14-16, 2004.

[19] Lane, C. and Axelrad, P., "Relative Semimajor Axis Uncertainty in High Earth Orbits," *Journal of Guidance, Control, and Dynamics*, Vol. 30, No. 6, 2007, pp. 1827-1830.